PHILOSOPHICAL TRANSACTIONS A

royalsocietypublishing.org/rsta

CC BY

Research

Cite this article: Seguel R *et al*. 2026 Tropospheric Ozone Assessment Report II: South America regional analysis. *Phil. Trans. R. Soc. A* **384**: 20250273.
https://doi.org/10.1098/rsta.2025.0273

Received: 30 December 2025
Accepted: 8 May 2026

One contribution of 8 to a theme issue 'Tropospheric Ozone Assessment Report II'.

Subject Areas:
atmospheric chemistry, atmospheric science

Keywords:
TOAR-II, South America, ozone distribution and trends, tropospheric column ozone, free troposphere, ozone precursors

Author for correspondence:
Rodrigo Seguel
e-mail: rodrigo.seguel@uc.cl

Tropospheric Ozone Assessment Report II: South America regional analysis

Rodrigo Seguel[1,2,3], Helen Worden[4], Kazuyuki Miyazaki[5,6], Tabish Ansari[7], Tim Butler[7,8], Charlie Opazo[1], Lucas Castillo[1], Daan Hubert[9], Viktoria Sofieva[10], Gaëlle Dufour[11] and Pablo Lichtig[12]

[1]Departamento de Química Inorgánica, Escuela de Química, Facultad de Química y de Farmacia and [2]Instituto para el Desarrollo Sustentable, Pontificia Universidad Católica de Chile, Santiago, Chile
[3]Center for Climate and Resilience Research (CR2), Chile
[4]Atmospheric Chemistry Observations & Modeling Laboratory (ACOM), NSF National Center for Atmospheric Research (NSF NCAR), Boulder, CO, USA
[5]Jet Propulsion Laboratory (JPL), California Institute of Technology, Pasadena, CA, USA
[6]Joint Institute for Regional System Science and Engineering (JIFRESSE), University of California Los Angeles, Los Angeles, CA, USA
[7]Research Institute for Sustainability at GFZ Helmholtz Centre for Geosciences, Potsdam, Brandenburg, Germany
[8]Institut für Meteorologie, Freie Universität Berlin, Berlin, Germany
[9]Royal Belgian Institute for Space Aeronomy (BIRA-IASB), Brussels, Belgium
[10]Finnish Meteorological Institute (FMI), Helsinki, Finland
[11]Université Paris Cité and Univ Paris Est Créteil, CNRS, LISA, 75013, France
[12]National Commission for Atomic Energy, Buenos Aires, Argentina

RS, 0000-0003-4641-5618; HW, 0000-0002-5949-9307; DH, 0000-0002-4365-865X

This study presents the first regional assessment of tropospheric ozone over South America for the early twenty-first century. We use observations from 14 combined satellite records, two atmospheric reanalyses, and model simulations to examine the spatial distribution, source contributions and trends in

Supplementary material is available online at https://doi.org/10.6084/m9.figshare.c.8640479.

THE ROYAL SOCIETY PUBLISHING

© 2026 The Authors. Published by the Royal Society under the terms of the Creative Commons Attribution License http://creativecommons.org/licenses/by/4.0/, which permits unrestricted use, provided the original author and source are credited.

Downloaded from royalsocietypublishing.org/rsta/article-pdf/doi/10.1098/rsta.2025.0273/6174208/rsta.2025.0273.pdf
by guest
on 09 November 2026

ozone and its precursors. Satellites and reanalysis data reveal enhanced tropospheric column ozone over the mid-latitudes of the west coast and the subtropical east coast, with 2005–2021 median values ($\pm 2\sigma$) ranging from 46 [±11] to 49 [±9] nmol mol^{-1}. By contrast, the lowest ozone levels occur over the northwest (39 [±8]–42 [±8] nmol mol^{-1}) and the southern cone (38 [±11]–40 [±7] nmol mol^{-1}). Tropospheric column ozone trends ($\pm 2\sigma$) differ across South America (2005–2021), reflecting substantial subregional and partial column variability. Satellite observations suggest an overall negative trend (low certainty), whereas reanalyses show positive trends with high certainty, ranging from +0.55 [±0.85] to +0.85 [±0.70] nmol mol^{-1} decade^{-1}. Model simulations identify global background methane as the dominant contributor to the South American tropospheric ozone burden, accounting for 41% (17 of 42 nmol mol^{-1}), followed by global anthropogenically emitted nitrogen oxides (31%). These findings improve our understanding of chemical processes and provide valuable inputs for assessing air quality and climate impacts.

This article is part of the theme issue 'Tropospheric Ozone Assessment Report II'.

1. Introduction

Ozone (O_3) is a fundamental trace gas in the atmosphere with multiple chemical roles that impact air quality and the climate system [1]. Changes in surface and vertical distribution can have profound impacts on health, ecosystems and climate forcing [2–4]. Compared with the Northern Hemisphere (NH), estimating ozone trends in the Southern Hemisphere (SH) has been more challenging owing to sparse observations and regionally produced emission inventories, which in turn affect the reliability of higher-level products such as chemical reanalysis [5]. Despite these limitations, observations of tropospheric column ozone in the southern mid-latitudes indicate medium confidence increases of less than 1 nmol mol^{-1} per decade since the mid-1990s [6,7]. Moreover, South America, a vast and diverse region extending from north of the Equator to Subpolar Patagonia (10°N to 55°S), is subject to multiple coupled dynamical and chemical processes influencing ozone distribution at the surface, in the free troposphere and upper troposphere, further complicating the determination of long-term ozone trends.

The second phase of the IGAC's Tropospheric Ozone Assessment Report (TOAR-II) established 17 focus working groups (WGs), which produced a set of contributing papers to support the preparation of the assessment papers. The South America regional assessment is one of the core papers comprising the assessment report, aiming to produce the first evaluation of tropospheric ozone distribution and trends over South America during the early twenty-first century.

(a) TOAR-II background and relevant literature

Our understanding of the influence of biomass burning, biogenic volatile organic compounds (VOCs) and stratosphere–troposphere exchange (STE) on ozone over South America is based in part on foundational knowledge gained from aircraft campaigns and ground-based observations conducted since the 1980s [8,9]. Building on this long-standing body of work, we focus here on key twenty-first-century contributions from TOAR-II and recent literature.

In South America, surface-level ozone measurements are primarily limited to urban agglomerations, with ozone exposure generally higher in extratropical than in tropical cities [10]. For the period 2017–2021, the present-day maximum daily 8 hour average (MDA8) metric in Santiago (mid-latitude) and São Paulo (subtropics) exceeded the short-term exposure of 51 nmol mol^{-1}, recommended by the World Health Organization (WHO), reaching 60.7 [± 5.5] and 61.3 [± 2.6] nmol mol^{-1}, respectively. By contrast, Bogotá and Quito, located in the tropics, showed lower short-term exposures of 42.8 [±3.6] and 38.6 [±1.9] nmol mol^{-1}, respectively. Similarly, peak-season exposure exceeded the WHO guideline of 31 nmol mol^{-1} in Santiago (40.9 [±2.9]) and São Paulo State (40.1 [±1.7]). Lower peak-season levels were again observed in Bogotá (26.4 [±3.1] nmol mol^{-1})

Downloaded from royalsocietypublishing.org/rsta/article-pdf/doi/10.1098/rsta.2025.0273/6174208/rsta.2025.0273.pdf
by guest
on 09 November 2026

Table 1. Trend reliability scale according to TOAR-II recommendations [12].

p-value	SNR value	term
$p \leq 0.01$	$SNR \geq 3$	very high certainty
$0.05 \geq p > 0.01$	$2 \leq SNR < 3$	high certainty
$0.10 \geq p > 0.05$	$1.65 \leq SNR < 2$	medium certainty
$0.33 \geq p > 0.10$	$1 \leq SNR < 1.65$	low certainty
$p > 0.33$	$SNR < 1$	very low certainty or no evidence

and Quito (26.7 [±1.1] nmol mol^{-1}). The relatively low ozone exposure in Bogotá and Quito is consistent with vertical ozone profiles measured by In-service Aircraft for a Global Observing System (IAGOS) and Southern Hemisphere ADditional OZonesondes (SHADOZ) networks over the South American tropics, where the 50th (5th) percentile was less than 40 nmol mol^{-1} (10 nmol mol^{-1}) from the surface to 200 hPa (700 hPa) [11].

Change points in the ozone trends have been detected in several South American cities [10]. In Santiago, the median ozone trend from 1997 to 2017 decreased at a rate of –0.19 [±0.04] nmol mol^{-1} yr^{-1} (very high certainty; see the trend reliability scale in table 1). After 2017, however, an increase of +0.62 [±0.44] nmol mol^{-1} yr^{-1} was observed over the last 5 years (with very high certainty), corresponding to an accumulated ozone of 3 nmol^{-1} (approx. 2017–2023). In São Paulo, the median ozone trend from 1998 to 2008 decreased at a rate of –0.17 [±0.23] nmol mol^{-1} yr^{-1} (very low certainty). After 2018, however, an increase of +0.31 [±0.23] nmol mol^{-1} yr^{-1} was detected over the subsequent 12 years (high certainty), corresponding to an accumulated increase of 4 nmol mol^{-1}. In Bogota, a flattened ozone trend in the 50th percentile was observed from 2008 to 2021 (very low certainty). In Quito, median ozone trends decreased from 2005 to 2011 at a rate of –0.22 [±0.21] nmol mol^{-1} yr^{-1} (high certainty), after which there was no further evidence of trend change.

The Harmonization and Evaluation of Ground-Based Instruments for Free Tropospheric Ozone Measurements (HEGIFTOM) focus WG reported tropospheric column ozone (TC-O_3) trends from the surface to 300 hPa at two northeastern sites based on ozonesonde data. The estimated trends (low certainty) were +0.40 [±0.78] at Paramaribo and +0.26 [±1.02] nmol mol^{-1} decade^{-1} at Natal [13]. Similarly, the Ozone and Precursors in the Tropics (OPT) focus WG applied a data-fusion approach using SHADOZ (San Cristóbal and Paramaribo) and IAGOS (primarily from Caracas and Bogotá) to assess ozone trends over northwestern South America between 1994 and 2019. The estimated trend was +0.47 [±0.79] nmol mol^{-1} decade^{-1} (medium confidence) [11]. Between 1998 and 2023, the Natal trend was significantly higher than between 1998 and 2019 [14]. However, for Paramaribo, the trend declined, shifting to slightly negative (with high confidence).

The Tropospheric Ozone Precursors focus WG, using Ozone Monitoring Instrument/Microwave Limb Sounder (OMI/MLS) data, estimated the TC-O_3 trends over South America between 2005 and 2019. Similar to the HEGIFTOM and OPT focus WGs, a positive trend was found in the tropics (0–30° S), while a negative trend was observed between 30 and 60° S [15]. Trends in tropospheric column nitrogen dioxide (TC-NO_2) derived from OMI, Global Ozone Monitoring Experiment-2 and SCanning Imaging Absorption spectroMeter for Atmospheric CHartographY (SCIAMACHY) data remain mostly low confidence, except in specific regions such as northern and central Chile and southern Brazil, where high-confidence increases were found. The tropospheric column carbon monoxide (TC-CO), based on daytime observations from Measurement of Pollution in the Troposphere (MOPITT), showed a South American trend of –0.14 [±0.09]% per year. Meanwhile, the tropospheric column formaldehyde (TC-CH_2O) exhibited increasing trends in Amazonia (central Brazil) and decreasing trends (with high confidence) in the southern half of South America.

Downloaded from royalsocietypublishing.org/rsta/article-pdf/doi/10.1098/rsta.2025.0273/6174208/rsta.2025.0273.pdf
by guest
on 09 November 2026

(b) Processes influencing South American ozone

Changes in ozone within the upper troposphere-lower stratosphere (UTLS) have a strong impact on atmospheric radiative forcing [16]. Over the mid-latitudes, STE can substantially contribute to upper-tropospheric ozone [17]. In the subtropical Andean, the Tololo site in Chile (2220 m.a.s.l.; 30.17° S, 70.80° W) stands out as one of the few high-altitude World Meteorological Organization (WMO) stations with a sufficiently long and continuous record to evaluate the impacts of STE. At this location, ozone increased at a rate of +0.29 nmol mol^{-1} yr^{-1} from 2006 to 2014 with a very high certainty [10]. This trend coincided with the global increase in methane (CH_4) following the plateau observed between 1999 and 2006 [18].

Moreover, the UTLS over South America is influenced by biomass burning events in South America, Australia and central Africa [19]. Plumes of biomass burning from central South America were detected in the UTLS during the SH Transport, Dynamics, and Chemistry (SouthTRAC) mission [20], while a cross-equatorial flux of biomass burning sources in central Africa was identified through modelling and measurements [21,22].

Background monitoring stations at pristine sites are even scarcer in southern South America. At Ushuaia (Argentina), consistent with previous work [6], low levels of surface ozone and a decreasing ozone trend have been reported, with high certainty and a low rate (−0.07 nmol mol^{-1} yr^{-1}) [10]. Over these latitudes, the early breakup of the stratospheric vortex in spring also affects the total column ozone [23], including the UTLS ozone [24]. Stratospheric sudden warming (SSW) events, which are rare events in the SH, are driven by gravity waves that can decelerate the westerly polar night jet and warm the polar stratosphere through descending motion. As a result, SSW events reduce the heterogeneous formation of active chlorine on polar stratospheric clouds, thereby limiting catalytic ozone depletion [25].

Hemispheric differences in UTLS ozone in air masses of stratospheric origin (300–200 hPa, 45–60° latitude) were investigated using *in situ* measurements from the High Altitude and Long Range research aircraft deployed during the September–November 2019 SouthTRAC mission. These observations were complemented by IAGOS commercial aircraft, ozonesonde records and the Copernicus Atmosphere Monitoring Service reanalysis data [24]. The comparative analysis of ozone mixing ratios showed lower ozone levels in the SH UTLS compared with the NH for the period 2002–2022. The SH UTLS median ozone was 54% of the NH counterpart during years with SSW disruptions and 57% during years without SSW. Intra-hemispheric ozone differences showed that in the NH, SSW years had a 9% ozone enhancement (31 [±11] nmol mol^{-1}) in the UTLS, whereas in the SH, the enhancement during SSW years reached 24% (43 [±13] nmol mol^{-1}).

(c) Rationale for this assessment

This research aims to enhance the understanding of regional processes that explain the distribution of and trends in tropospheric column ozone and its precursors. To address information gaps across South America, we used satellite observations, reanalysis products and models with ozone source-attribution capabilities in coordination with TOAR-II focus WGs. First, a TC-O_3 dataset combining 14 harmonized satellite records [26] was compared with reanalysis data. Second, based on the evaluation of the Chemical Reanalysis focus WG [5], two reanalyses were applied to unmonitored regions: CAMSRA and the second-generation Tropospheric Chemistry Reanalysis (TCR-2). Third, we assessed the contribution of nitrogen oxides (NO_x) and reactive carbons (RCs) (CO, CH_4 and VOC) from various sources to South American regional ozone using the Community Atmosphere Model version 4 with chemistry (CAM4-Chem) simulations enabled with an ozone tagging mechanism [27–29]. Thus, we characterize the distribution of ozone and its precursors, identify their sources, report trends with associated uncertainties and provide policy-relevant key messages.

Downloaded from royalsocietypublishing.org/rsta/article-pdf/doi/10.1098/rsta.2025.0273/6174208/rsta.2025.0273.pdf
by guest
on 09 November 2026

2. Data and model (or assimilation) products

In this section, we provide relevant information associated with satellites, chemical reanalysis and global chemical transport model simulations to facilitate a better understanding of the results.

(a) Combined satellite data

We used a tropospheric ozone product that combines observations in 14 harmonized satellite records [26]. The complete list of satellites and measurement techniques used to retrieve ozone is provided in table S1 in the supplementary material. The resulting time series (2005–2021) provides monthly mean TC-O_3 on a 5 × 5° grid in nmol mol^{-1} between the surface and the thermal tropopause, estimated from MERRA-2 (Modern-Era Retrospective Analysis for Research and Applications, Version 2) (see §2b).

(b) Reanalysis products: CAMSRA, TCR-2 and MERRA-2

We used mixing ratios of ozone, nitric oxide (NO), NO_2, CO, CH_2O and CH_4 obtained from the chemical reanalysis CAMSRA [30]. We studied the period from 2005 to 2021, except for methane, for which data are available up to 2020 [31]. Note that CH_4 was analysed in a reanalysis system separate from the one used for the other species. Therefore, chemical interactions between CH_4 and the short-lived species were not treated in a fully coupled manner, which may limit the strict interpretation of coupled chemical budgets and trend attribution in our study. Columns of ozone, NO, NO_2, CO and CH_2O were also obtained from TCR-2 [32]. Table 2 summarizes the resolution, the observation assimilated, the inventories used and the meteorological inputs.

We used the WMO first thermal tropopause estimated from the MERRA-2 reanalysis, with a horizontal resolution of 0.5° lat. × 0.625° lon. and a time resolution of 3 hours [43]. These data are available in a public data repository at Forschungszentrum Jülich (https://datapub.fz-juelich.de/slcs/tropopause/).

(c) CAM4-Chem global model output with NO_x and VOC tagging

We use model-derived monthly mean tropospheric ozone mixing ratios, along with various tagged NO_x and VOC precursor contributions from tagging-enabled CAM4-Chem global model simulations, for the 2000–2018 period. The CAM4-Chem model and the TOAST1.0 tagging system used in the simulations have been described previously in the literature [27,44]. The model is run with the Model for OZone And Related chemical Tracers chemical mechanism [45] and uses the newly released Hemispheric Transport of Air Pollution version 3 inventory for the anthropogenic emissions [38] and the CAMS-GLOB-BIO inventory for biogenic emissions [40]. Table 2 summarizes key information, including inventories used and their references. Further descriptions of the model settings and inputs, as well as ozone evaluations, are available for various world regions [28,29].

The CAM4-Chem simulation period (2000–2018) does not fully overlap with the satellite and reanalysis data (2005–2021), which should be considered when comparing these datasets. Nevertheless, a key strength of the simulation lies in its tagging capability, which allows ozone to be attributed separately to NO_x and VOC precursors. In the NO_x-tagged framework, attribution is independent of VOC origin and vice versa for VOC-tagged simulations, thereby providing additional insight into the interpretation of ozone trend estimates.

Downloaded from royalsocietypublishing.org/rsta/article-pdf/doi/10.1098/rsta.2025.0273/6174208/rsta.2025.0273.pdf
by guest
on 09 November 2026

Table 2. Resolution, assimilated data and inputs used by the reanalysis and CAM4-Chem model.

product / data	horizontal, vertical and temporal resolution	species assimilated	emission inventory used	meteorological inputs
CAMSRA	0,75°, 60 layers from surface to 0.1 hPa, 3 h	O_3 (SCIAMACHY, MIPAS[(a)], MLS, OMI, GOME-2, SBUV/2[(b)], NO_2 (OMI, SCIAMACHY, GOME-2), CO (MOPITT)	MACCity [33]; GFASv1.2 [34]; MEGAN2.1 [35]	ERA-5
TCR-2	1.125° x 1.125°, 32 levels from surface to 4 hPa, 6 h	O_3 (MLS, TES[(c)]), NO_2 (OMI, SCIAMACHY, GOME-2), HNO_3 (MLS), CO (MOPITT)	HTAPv2 for anthropogenic emissions [36]; GEIA for NO_x (from soil) [37]; GFED-v4 inventory for biomass burning emissions	ERA-Interim
CAM4-Chem	1.9° x 2.5°, 56 vertical levels on the hybrid sigma-pressure coordinate with model top at approximately 1.86 hPa, 0.5 h	No assimilation of ground observations or satellite data for chemical species. CH_4 is prescribed as lower boundary conditions and O_3, NO, NO_2, HNO_3, CO, CH_4 and N_2O are prescribed/assimilated as upper boundary conditions	HTAPv3 (2000-2018) [38]; GFED-v4 [39]; CAMS-GLOB-BIO-v3.0 for biogenic emissions [40], and biogenic NO_x (from soil) is prescribed as in [41]	MERRA2 reanalyses [42]. Temperature, horizontal winds, and sensible and latent heat fluxes from MERRA2 reanalysis dataset are nudged every time step (30 min) by 10% towards analysis fields

(a) MIPAS: Michelson Interferometer for Passive Atmospheric Sounding, (b) SBUV: Solar Backscatter Ultraviolet and (c) TES: Tropospheric Emission Spectrometer.

3. Methods

In this section, we explain how we used the available data to analyse the tropospheric and partial columns of ozone and its precursors.

(a) Determination of tropospheric columns and tropospheric partial columns

Chemical reanalysis data products, created through the long-term assimilation of multiple satellite observations (table 2), provide an observationally constrained, continuous record of atmospheric composition on a global scale. This approach helps to fill gaps in the current observing system and is expected to provide unique insights into regions with sparse *in situ* networks, such as South America.

We determined the TC from the surface to the first thermal tropopause. We also distinguish the lower (LTC), middle (MTC) and upper tropospheric columns (UTC), considering the intervals from the ground to 700 hPa, 700 to 300 hPa and 300 hPa to tropopause, respectively. In those cases where the tropopause was found within the MTC, the upper limit considered was the tropopause, and therefore, the UTC was discarded. When the surface pressure was lower than 700 hPa, the LTC was discarded, and the MTC was calculated from the surface pressure up to 300 hPa (or the tropopause). Finally, when the tropopause was not identified, both the MTC and UTC were discarded.

Downloaded from royalsocietypublishing.org/rsta/article-pdf/doi/10.1098/rsta.2025.0273/6174208/rsta.2025.0273.pdf
by guest
on 09 November 2026

The TCR-2 and MERRA-2 chemical species, as well as the tagging obtained from CAM4-Chem, were bilinearly interpolated onto the CAMSRA grid owing to the higher horizontal resolution of the latter. The vertical integration average was then obtained using equation (3.1), where p is the pressure, P_{upper} and P_{lower} are vertical boundaries of the tropospheric layer, r is the volume mixing ratio of the chemical species and TC_r is the tropospheric column of the species r:

$$TC_r = \frac{1}{P_{\text{lower}} - P_{\text{upper}}} \int_{P_{\text{lower}}}^{P_{\text{upper}}} r dp. \tag{3.1}$$

In the following, the terms 'tropospheric column' and 'tropospheric partial columns' are used to denote their corresponding column-averaged mixing ratios.

(b) Satellites and chemical reanalysis

The combined satellite record used in this study does not provide tropospheric partial columns or ozone precursor columns. Therefore, the TC-O_3 from combined satellites is primarily used to inform the agreement with reanalysis and tagged models. When comparing with higher-resolution reanalysis data, it is important to consider the coarse horizontal resolution of the combined satellite data ($5 \times 5°$). This is particularly relevant over the Andes, where averaging across strong elevation gradients can lead to larger differences.

The application and interpretation of reanalysis in South America require considering the following aspects. Both CAMSRA and TCR-2 showed reasonable agreement with ozonesonde observations in the middle and upper troposphere over the SH (20–60°S), with temporal correlations of approximately 0.75 at 250 hPa and 0.8 at 500 hPa during 2006–2016 [5]. At 250 hPa, the mean bias was 4 nmol mol^{-1} in TCR-2 and 7 nmol mol^{-1} in CAMSRA, with a standard deviation of about 14 nmol mol^{-1} in both datasets. At 500 hPa, the mean bias was nearly zero in TCR-2 and –4 nmol mol^{-1} in CAMSRA, while the standard deviation was about 6 nmol mol^{-1} in both datasets. Overall, both reanalyses reproduced SH ozone variability well [5].

Based on reanalysis performance, CAMSRA and TCR-2 can be useful for studying the middle and upper troposphere. The higher correlation found in the mid-latitudes compared with tropical South America may reflect the better representation of dominant large-scale synoptic processes in meteorological reanalysis than of dominant convective processes in tropical regions [5]. The discrepancy between the reanalysis products is larger at the surface than in the free troposphere, with TCR-2 showing higher surface ozone than CAMSRA over South America.

(c) Tagged simulations

Model-simulated ozone mixing ratios from the TOAST1.0 tagging system can be broken down separately into various contributions from NO_x sources and RC sources (including CH_4), respectively [29,46]. To provide an unambiguous attribution of ozone to its emitted precursors, two separate model runs are performed, attributing the total tropospheric ozone fully to its NO_X sources (including the stratosphere) and fully to its VOC sources (including methane and the stratosphere) [27].

(d) Regional clustering

Monthly time series were calculated from the TC-O_3 at hourly resolution (3 h CAMSRA and 6 h TCR-2) for all grid cells. K-means clustering was then applied to identify four groups, using the elbow method to determine the optimal number of clusters. Overall, the four-cluster solution offers an optimal compromise, preserving consistent regional patterns across tropospheric partial columns and seasons. Figure 1a depicts the boundaries of the four zones.

Downloaded from royalsocietypublishing.org/rsta/article-pdf/doi/10.1098/rsta.2025.0273/6174208/rsta.2025.0273.pdf
by guest
on 09 November 2026

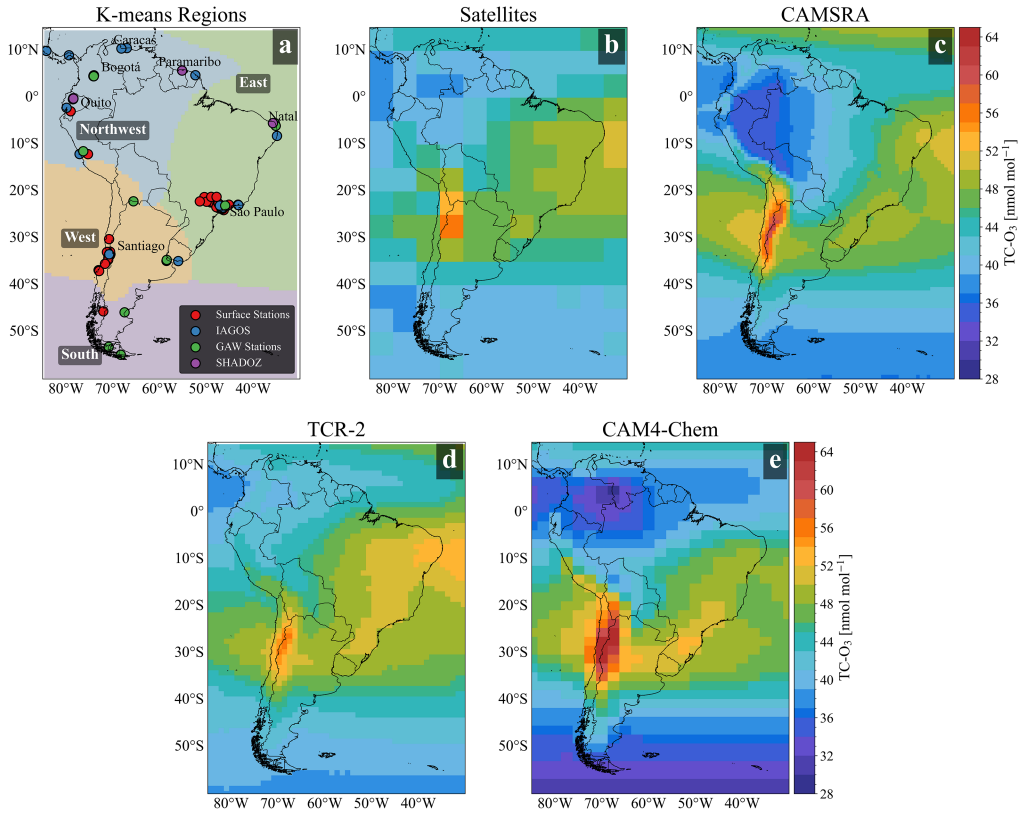


Figure 1. Tropospheric column ozone over South America. Panel (a) shows four subregions obtained from the application of K-means to tropospheric column ozone provided by CAMSRA and TCR-2. In panel (a), red dots indicate locally managed surface monitoring stations, green dots indicate stations of the GAW program, blue dots correspond to sites associated with IAGOS data and purple dots indicate SHADOZ stations. Panel (b) shows the mean tropospheric column ozone in nmol mol^{-1} obtained from the combined satellites for the period 2005–2021. Panels (c)–(e) show the same information described in panel (b) for the CAMSRA reanalysis, TCR-2 and CAM4-Chem (2005–2018), respectively. In panel (a), some cities are indicated for reference.

(e) Trend estimations

We applied the quantile regression method to estimate trends based on monthly anomalies, as recommended by TOAR-II guidelines [12]. First, we calculated monthly deseasonalized anomalies with respect to a climatology obtained from monthly harmonics (of 12 and six months). Then, we applied quantile regression to estimate trends in medians of time series. Finally, we applied a moving-block bootstrap algorithm to estimate uncertainty in trends influenced by autocorrelation in time series. Confidence intervals quantify how precisely the median trend can be estimated. Table 1 presents the calibrated language adopted, which combines the p-value and signal-to-noise ratio (SNR) to provide a more robust assessment of trend significance and strength, with the SNR reflecting the magnitude of the trend relative to its uncertainty.

4. State of tropospheric ozone in South America

In this section, we characterize the state of tropospheric ozone in South America for the early twenty-first century (up to 2021) in terms of its horizontal and vertical distribution, precursors, including stratospheric contribution, and trends and uncertainties using a calibrated language.

Downloaded from royalsocietypublishing.org/rsta/article-pdf/doi/10.1098/rsta.2025.0273/6174208/rsta.2025.0273.pdf
by guest
on 09 November 2026

(a) Tropospheric ozone distribution

Ozone measurements in South America rely on *in situ* surface measurements and ground-based (ozonesondes and remote sensing techniques), including the latter IAGOS commercial aircraft measurements. Existing measurement sites are shown in figure 1a to highlight the critical role of reanalyses in areas with sparse *in situ* observations. Figure 1b–e show the TC-O_3 of combined satellites, CAMSRA, TCR-2 and CAM4-Chem, while figure S1 in the supplementary material shows the bias of combined satellite data with respect to reanalysis and CAM4-Chem. We noted that TCR-2 fits the combined satellite data better than CAMSRA and CAM4-Chem. Roughly, the disagreement tends to be higher over elevated terrain, with satellites being higher over the tropical Andes region and lower over the mid-latitude Andes region. This difference may (at least partially) be a result of the different horizontal resolution. Additionally, combined satellite observations are higher than those from reanalysis and tagged models over southern South America.

Four ground-based observations available in the tropics (Natal, Paramaribo, Bogotá and Caracas) were used to further evaluate reanalysis and model results (supplementary material, table S2). In general, the reanalysis showed higher partial columns than ground-based observations over these sites, with better agreement in the mid-troposphere. Differences in the MTC-O_3 were less than 20%. Conversely, CAM4-Chem columns tended to be lower than ground-based observations, without a consistent bias pattern. Differences of less than 13% were observed in the mid-troposphere.

To improve clarity, results are first presented in terms of regional differences based on TC-O_3, followed by their vertical structure and seasonal variability.

(i) Subregional distribution of O_3

Based on the TC-O_3 of both reanalyses, four subregions are defined: northwest, east, west and south of South America (Figure 1a). These subregions exhibit distinct ozone patterns. According to CAMSRA, the lowest TC-O_3 medians ($\pm 2\sigma$) were found in the south and northwest with average columns of 38 [±11] and 39 [±8] nmol mol^{-1}, respectively, while the highest TC-O_3 levels were found in the east and west South America with 46 [±11] and 47 [±13] nmol mol^{-1}. Table S3 in the supplementary material summarizes the TC-O_3 obtained from the combined satellite data, reanalysis and the tagged model by subregion.

(ii) Vertical structure of O_3

After establishing the regional distribution of TC-O_3, we examine the vertical structure of ozone to better understand the processes driving these patterns. The LTC-O_3 showed higher levels over the subtropics, both on the west and east coasts of South America. The MTC-O_3 showed higher values over the South Atlantic Ocean and the eastern part of South America. In turn, the UTC-O_3 showed the influence of the stratosphere over high latitudes and mid-latitudes, with the latter above the Andes Mountain range (supplementary material, figure S2).

(iii) Seasonal variability

Given the reanalysis performance discussed in §3c, the seasonal analysis focuses on MTC and TC. These columns exhibit a clear seasonality across South America (figure 2), with ozone levels peaking in September and reaching a minimum in April. The eastern and western subregions record the highest TC-O_3 and MTC-O_3 values in September and October, respectively, while the southern region shows the lowest levels in February. The seasonality derived from the combined satellites, reanalysis and the tagged model is shown in figure S3 in the supplementary material.

The spatial distribution of ozone precursors is broadly consistent with the regional patterns described above. Figure 2 indicates that CO mixing ratios are highest in the northwest, followed

Downloaded from royalsocietypublishing.org/rsta/article-pdf/doi/10.1098/rsta.2025.0273/6174208/rsta.2025.0273.pdf
by guest
on 09 November 2026

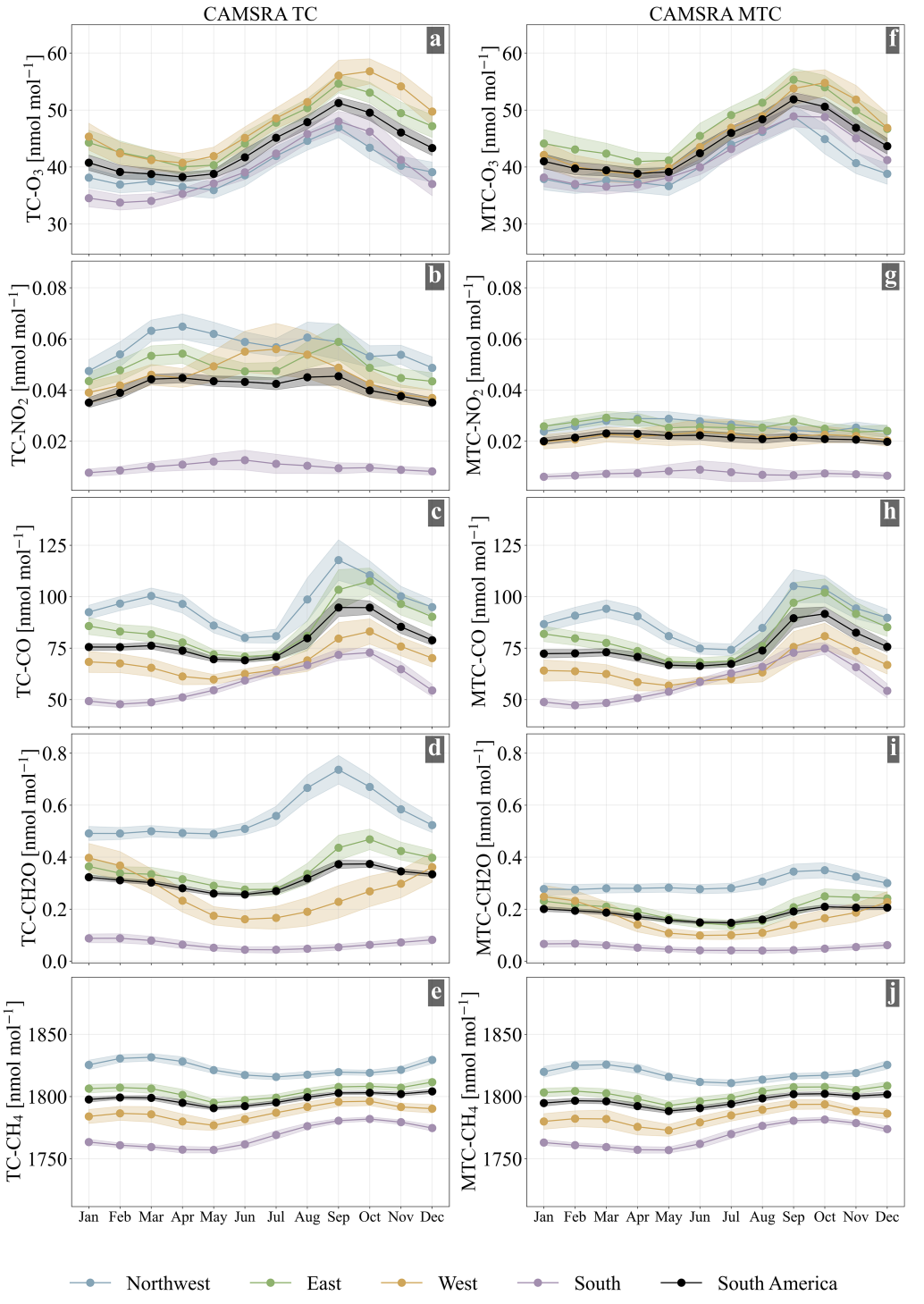


Figure 2. Monthly means of (total) tropospheric columns and middle tropospheric columns for CAMSRA chemical species for the period 2005–2021 (except methane: 2005–2020). The panels (a)–(e) show the total tropospheric column (TC) for O_3, NO_2, CO, CH_2O and CH_4, respectively. The panels (f)– (j) show the same species for the middle tropospheric column (MTC). Colours indicate the northwest, east, west, south and entire South America. Shaded areas denote the 95% confidence intervals.

Downloaded from royalsocietypublishing.org/rsta/article-pdf/doi/10.1098/rsta.2025.0273/6174208/rsta.2025.0273.pdf
by guest
on 09 November 2026

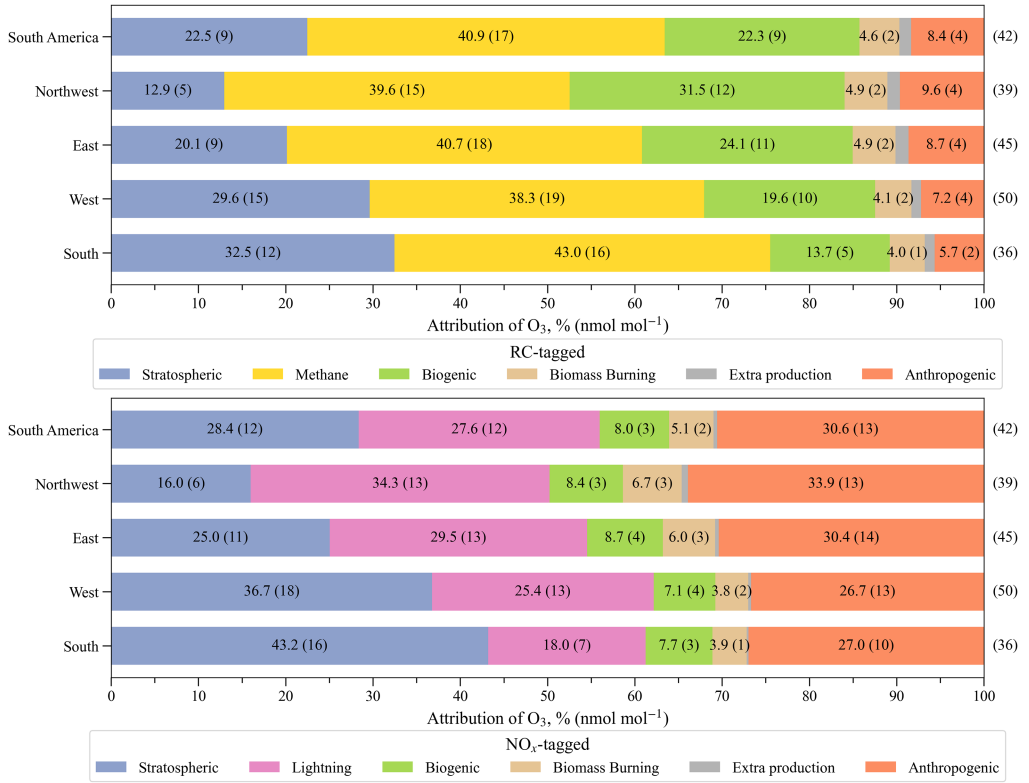


Figure 3. Attribution of tropospheric column ozone to RC-tagged and NO_x-tagged precursor emission in South America and its subregions based on the Cam4-Chem model for the period 2005–2018. The upper and lower panels show RC-tagged and NOx-tagged, respectively. Percentage contribution and absolute contribution in nmol mol^{-1} (in parentheses) are indicated in each bar. To the right of each bar, the simulated (total) tropospheric column ozone for South America and its subregions is shown in parentheses.

by the east. NO_2 levels are lower in the MTC than in the TC-NO_2, reflecting contributions from large urban agglomerations and, to a lesser extent, enhanced abundance in the upper troposphere (supplementary material, figure S5). CH_2O presents higher TC-CH_2O and MTC-CH_2O values in the northwestern and eastern regions relative to the western and southern ones. Tropospheric partial column values indicate an important surface origin for CH_2O (supplementary material, figure S7). By contrast, CH_4 shows similar levels in TC-CH_4 and MTC-CH_4 owing to its longer atmospheric lifetime, with column values decreasing from low to high latitudes.

Interestingly, a closer look at the TC-CH_4 reveals CH_4 enhancements in oil and natural gas production zones, including those in Colombia, Venezuela, Ecuador, Bolivia and Brazil (supplementary material, figure S8). In the Chile case, on the other hand, a country with minimal natural gas production, we observe an important enhancement over the Santiago metropolitan region, which introduced natural gas on a large scale in 2009 to effectively reduce particulate matter [10,47]. The widespread consumption of natural gas in Santiago suggests a significant role of methane in the high ozone enhanced over this city.

(b) Source attribution of tropospheric ozone

The stacked bar chart shows the TC-O_3 over South America and its sub-regions simultaneously attributed to NO_x and VOC emissions from different sectors and world regions (figure 3). From a VOC-attribution perspective, TC-O_3 over South America is dominantly attributed to background

Downloaded from royalsocietypublishing.org/rsta/article-pdf/doi/10.1098/rsta.2025.0273/6174208/rsta.2025.0273.pdf
by guest
on 09 November 2026

CH_4 (approx. 40%), followed by global biogenic VOCs (including carbon monoxide, isoprene, monoterpenes and methanol) and stratospheric source, with the latter two reaching approximately 22%. From a NO_x attribution perspective, global anthropogenic sources, lightning and stratospheric contributions stand out, with a relatively equal contribution (approx. 30%), while NO_x from biogenic plus biomass burning sources accounts for approximately 13%.

It is worth noting that ozone attributed to stratospheric production in the NO_x-tagged simulation is greater than the stratospheric component from the RC-tagged simulation (figure 3). This is owing to the production of NO_x from the oxidation of nitrous oxide (N_2O), primarily in the stratosphere, which is then transported into the troposphere, where it can contribute to ozone production [27].

Furthermore, we emphasize that the influence of NO_x from sources outside South America does not represent the direct transport of NO_x itself, as its atmospheric lifetime is generally too short to reach the region. Rather, it reflects enhanced ozone production in upwind regions, with ozone being transported to South America, as its lifetime is sufficiently long, particularly via free-tropospheric pathways and subsequent mixing into the boundary layer. A detailed regional source attribution is beyond the scope of this study.

The subregional picture shows that the higher CH_4 abundance in the northwest (figure 2e) does not imply higher ozone mixing ratio from CH_4 oxidation; here, the CH_4 contribution to ozone reaches an average of 15 nmol mol^{-1}, slightly lower than other subregions (figure 3), suggesting a lower importance of CH_4 in ozone formation in regions where biogenic VOC is abundant [29]. Instead, the CH_4 contribution to ozone is higher (and BVOC contribution lower) in western South America (19 nmol mol^{-1}), followed by the eastern (18 nmol mol^{-1}) and the southern subregions (16 nmol mol^{-1}) (figure 3).

Ozone attributed to biogenic VOCs in RC-tagged simulations is more prominent in the northwest and east, whereas stratospheric contributions are larger in the western and southern subregions. Regarding NO_x-tagged simulations, the stratospheric transport is much higher in the western/southern subregions than in the northwestern/eastern subregions.

The analysis of the partial tropospheric columns also shows some variations with respect to the total tropospheric column (supplementary material, figures S9-S11). These differences are primarily driven by higher CH_4 and anthropogenic NO_x contributions in the LTC (supplementary material, figure S9), whereas in the UTC, a strong influence of stratospheric ozone transport is evident in RC-tagged and NO_x-tagged simulations (supplementary material, figure S11). On the other hand, the MTC resembles the TCO.

(c) Chemical processes interpretation

CO exhibits a broadly similar seasonal pattern, except in the northwest, where two maxima occur in September and March (TC-CO and MTC-CO), the latter corresponding to the biomass burning season in northwestern South America (dry season in the Colombian Andes and wet season in the central Andes). Interestingly, only one of these two maxima coincides with the September CH_2O maximum, a species emitted biogenically and from biomass burning, which can be modulated by relative humidity [48]. In western South America, the CO lifetime differs, with a maximum in austral winter driven by high anthropogenic emissions.

From CAMSRA, we identified elevated methane levels over western Amazonia and the central Andes, partly associated with strong wetland CH_4 emissions, as previously reported [49]. In this region, CH_2O abundances are notably higher during the second half of the year (figure 4). Furthermore, CAM4-Chem simulations indicate that biogenic sources contribute more to CH_2O than CH_4 oxidation (supplementary material, figure S12), particularly over western Amazonia and the central Andes during this period. By contrast, CH_2O originating from CH_4 oxidation is relatively more important in the northwest and eastern regions.

Figure 4 presents regional distributions of ozone attributed to CH_4, stratospheric influence and anthropogenic NO_x, clearly identifying the subregions where CH_4, STE and NO_x contribute significantly to ozone formation. In a significant portion of the northwestern subregion, despite

Downloaded from royalsocietypublishing.org/rsta/article-pdf/doi/10.1098/rsta.2025.0273/6174208/rsta.2025.0273.pdf
by guest
on 09 November 2026

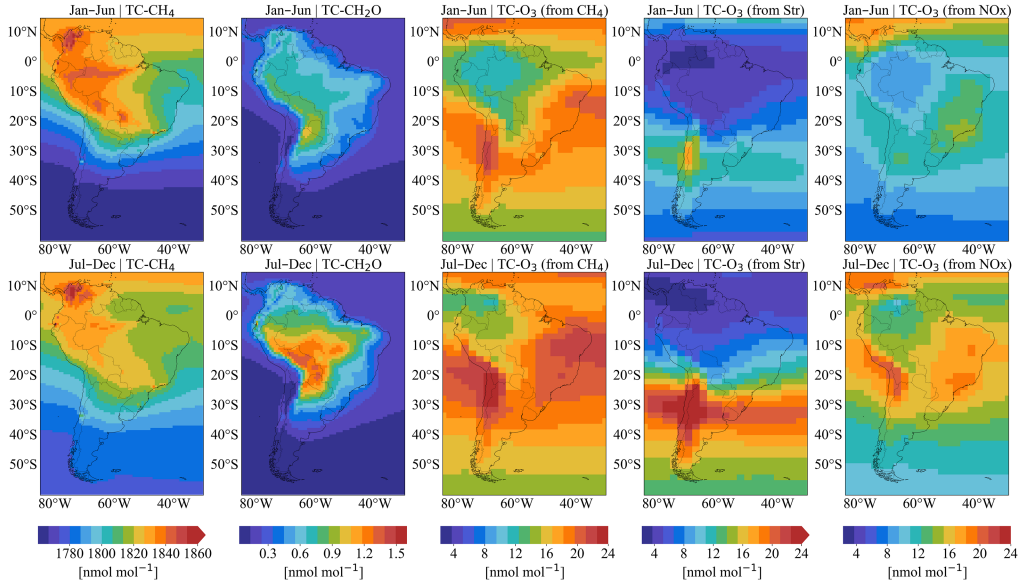


Figure 4. Tropospheric column methane (2005–2020) and formaldehyde (2005–2021) obtained from CAMSRA reanalysis and tropospheric column ozone owing to methane, from stratospheric origins and anthropogenic nitrogen oxides, as simulated by Cam4-Chem for the first (January–June) and second (July–December) semesters for the period 2005–2018.

high methane availability and enhanced formaldehyde production from biogenics, ozone levels remain relatively low owing to the limited availability of NO. Ozone formation driven by anthropogenic NO_x is instead confined to urban agglomerations in the northwest, east and west.

Overall, in the convective northwest, where ozone photolysis (λ less than 336 nm) also represents a dominant sink, the presence of additional ozone precursors, such as lightning NO_x, methane and biogenic volatile organic compounds, does not necessarily translate into elevated ozone levels. By contrast, in the western and eastern subregions influenced by the South Pacific and South Atlantic anticyclones, *in situ* ozone formation via NO_2 photolysis is more efficient, with important implications for air quality and human health.

(d) Trends in ozone and its precursors

In the following section, we assess trends in ozone and its precursors across South America. We used existing tropospheric ozone products, acknowledging their respective strengths and uncertainties without assigning any as a definitive reference.

(i) Tropospheric ozone trends

TC-O_3 derived from combined satellites declines between 2005 and 2021 with low certainty over South America. By contrast, we observe consistency between the positive TC-O_3 trends obtained from CAMSRA and TCR-2 (figure 5). We also note the same consistency between the TC-O_3 trend simulated using CAM4-Chem and the trends determined by the reanalyses. The confidence interval associated with the mean TC-O_3 trends in South America is relatively large owing to the variability between the subregions and partial columns.

In the northwest, CAMSRA shows a TC-O_3 trend ($\pm 2\sigma$) of +0.85 [±0.70] nmol mol^{-1} decade^{-1} (high certainty), while TCR-2 indicates a positive trend with low certainty; together, these reanalysis-based estimates are consistent within uncertainties and broadly agree with previously reported positive trends over northern and tropical South America. The combined satellite data, in turn, show no evidence for the TC-O_3 trend. At this point, the monthly time series provides

Downloaded from royalsocietypublishing.org/rsta/article-pdf/doi/10.1098/rsta.2025.0273/6174208/rsta.2025.0273.pdf
by guest
on 09 November 2026

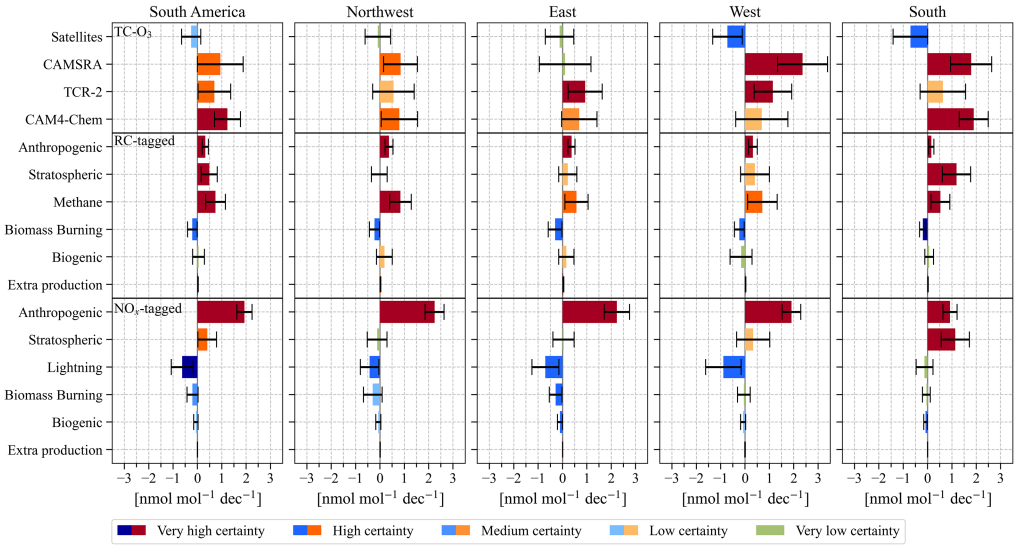


Figure 5. Tropospheric column ozone trends (2005–2021) and tropospheric column ozone attributed to RC-tagged and NO_x-tagged simulation using CAM4-Chem (2005–2018) by subregion in South America. Error bars show confidence interval (±2 sigma). Colours indicate reliability.

additional insights into these divergent trends. From figure S16 in the supplementary material, we observed that the combined satellite seasonal maxima were higher than those of the reanalysis, especially at the beginning of the time series. While this difference tended to even out over time, TCR-2 also showed an increase of a second maximum in the reanalysis data at the end of each year.

The greatest difference between the two reanalyses is observed in the east, where the CAMSRA trend is flat with very low certainty, and TCR-2 shows a positive trend of +0.93 [±0.70] nmol mol^{-1} $decade^{-1}$, with very high certainty. Also, in this region, there is no evidence for a TC-O_3 trend in the combined satellite time series. The monthly time series reveals that the primary difference between the reanalysis and the combined satellites lies in the more intense seasonal minima recorded by the latter (supplementary material, figure S17). A clear second maximum increase over time was also observed in TCR-2.

A very high certainty upward trend in TC-O_3 is observed in the west, where CAMSRA and TCR-2 show trends of +2.4 [± 1.0] and +1.1 [±0.8] nmol mol^{-1} $decade^{-1}$, respectively. By contrast, combined satellites show a decrease of –0.72 [±0.60] nmol mol^{-1} $decade^{-1}$ (high certainty). Examination of the monthly time series showed a better fit in the west during the first part of the time series (supplementary material, figure S18). Subsequently, the maxima were higher in the reanalysis data, and the minima were lower in the combined satellite data. This pattern was more pronounced in CAMSRA.

In the south, CAMSRA shows a positive trend of +1.8 [±0.85] nmol mol^{-1} $decade^{-1}$ with very high certainty, whereas the positive trend associated with TCR-2 has low certainty. Combined satellites show a decrease of –0.70 [±0.71] nmol mol^{-1} $decade^{-1}$ (high certainty). Here, at the beginning of the time series, CAMSRA exhibited lower minima than the combined satellites, and at the end of the time series, it showed higher maxima than the satellites (supplementary material, figure S19). In the case of TCR-2, higher seasonal minima were observed compared with those in the satellite data.

The TC-O_3 trend determined from CAM4-Chem simulations shows positive trends in the northwest and south, with high and very high certainty, respectively. Additionally, in these two subregions, CAM4-Chem exhibits similar trends to those of CAMSRA.

Downloaded from royalsocietypublishing.org/rsta/article-pdf/doi/10.1098/rsta.2025.0273/6174208/rsta.2025.0273.pdf
by guest
on 09 November 2026

The trend in TC-O_3 produced by RC-tagged shows a positive rate for stratospheric ozone in the south, while trends with low certainty are observed in the east and west. The trend in the northwest is flat for the stratospheric contribution.

Ozone produced from CH_4 oxidation shows positive trends across all subregions with an average rate in South America of +0.74 [±0.40] nmol mol^{-1} $decade^{-1}$, with very high certainty. The highest trend is observed in the northwest at +0.84 [±0.44] nmol mol^{-1} $decade^{-1}$. Western South America shows the highest rate of +0.81 [±0.28] nmol mol^{-1} $decade^{-1}$ (very high certainty) in the LT, while the northwest, on the other hand, shows the highest rate of +1.0 [±0.61] nmol mol^{-1} $decade^{-1}$ (very high certainty) in the MT.

The anthropogenic VOC contribution to TC-O_3 in South America shows an increasing rate of +0.32 [±13] nmol mol^{-1} $decade^{-1}$ with very high certainty. TC-O_3 produced by VOCs emitted from global biomass burning exhibits negative trends in all subregions with high or very high certainty, averaging –0.21 [±0.20] nmol mol^{-1} $decade^{-1}$ in South America. For its part, TC-O_3 produced from global biogenic VOCs presents low or very low certainty in trends.

Anthropogenic NO_x contribution largely drives the positive TC-O_3 trend in South America, with a regional mean of +1.9 [±0.31] nmol mol^{-1} $decade^{-1}$. This contribution is slightly lower in the south, where a stronger stratospheric influence is also observed. In the remaining subregions, the stratospheric contribution to the trends has low or very low confidence. By contrast, the contribution of lightning to the TC-O_3 trend is negative in the northwest, east and west. In particular, the negative values in the east and west indicate a pronounced decline. Although lighting is an important ozone source through photochemical production, contributing up to 12 nmol mol^{-1} over South America (figure 3), its decreasing trend may be linked to changes in deep convection. These changes affect both the lofting and dilution of ozone, on the one hand, and the accumulation of ozone precursors, on the other [50]. We also detected a robust downward trend in ozone contributions from lightning over the northwest upper troposphere of –1.1 [±0.71] nmol mol^{-1} $decade^{-1}$ (very high certainty), where the ozone owing to lightning reached 22 nmol mol^{-1} (supplementary material, figure S11). Finally, the contribution of NO_x from biomass burning and biogenic sources (from soils) shows negative TC-O_3 trends, although with low or very low certainty.

(ii) Ozone precursor trends

CAMSRA indicates a downward trend in TC-NO and TC-NO_2 with very high certainty (figure 6). This decrease is primarily driven by processes occurring in the upper troposphere, and to a lesser extent, in the middle troposphere (supplementary material, figures S22 and S23). By contrast, the comparison between CAMSRA and TCR-2 for the LTC-NO and LTC-NO_2 reveals divergent trends, i.e. negative in CAMSRA and positive in TCR-2 (supplementary material, figure S21). The latter is reflected in the mean TC-NO_2 over South America.

The upward trend in TC-CH_2O is consistent between both reanalyses. In South America, the TC-CH_2O trend (high certainty) indicates an increase in photochemical activity, which is not necessarily associated with the upward trend in TC-O_3. This trend is driven by biogenic emissions in the northwest (west Amazonia and central Andes), particularly in the lower and middle troposphere, as described in §4c. In the upper troposphere, however, the TC-CH_2O trend is generally negative or associated with very low certainty.

Among the ozone precursors, trends in TC-CO show the greatest uncertainty. Both reanalyses report very low (CAMSRA) and low certainty (TCR-2). In figure 6, we can see the wide confidence interval associated with CO trends. By contrast, the clearest precursor trend is CH_4. The TC-CH_4 trend estimated from CAMSRA (2005–2020) shows a robust positive trend of +66 [±4.6] nmol mol^{-1} $decade^{-1}$ (very high certainty). The upward trends with very high certainty are observed across all South American subregions. The highest rate occurs in the northwest (+69 [±4.0] nmol mol^{-1} $decade^{-1}$), followed by the east and west (+67 [±3.7] and +67 [±3.9] nmol mol^{-1} $decade^{-1}$, respectively) and the south (+61 [±6.4] nmol mol^{-1} $decade^{-1}$).

Downloaded from royalsocietypublishing.org/rsta/article-pdf/doi/10.1098/rsta.2025.0273/6174208/rsta.2025.0273.pdf
by guest
on 09 November 2026

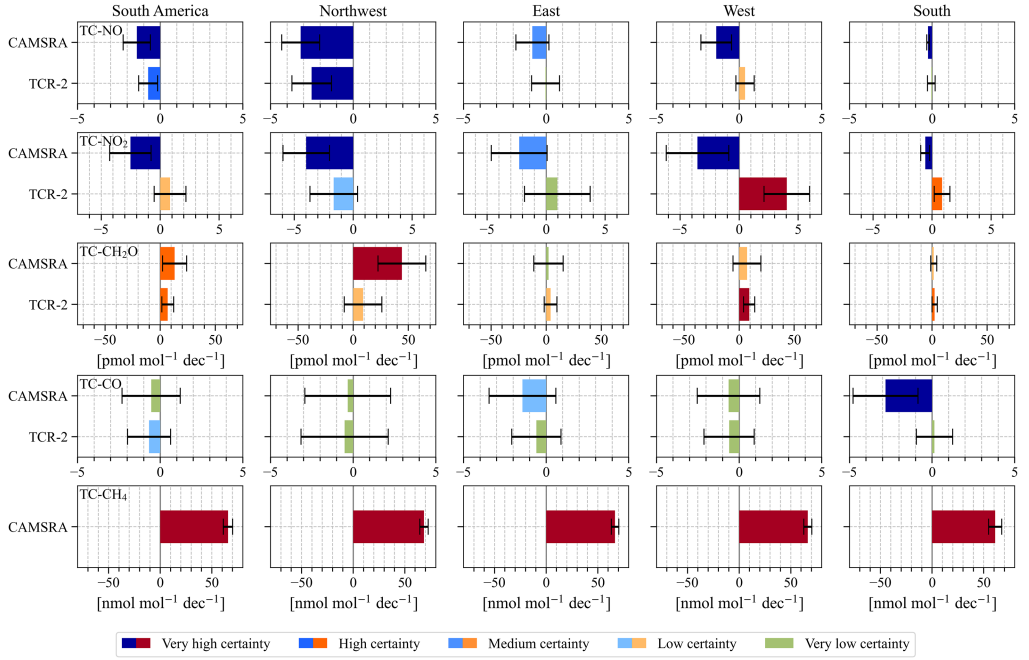


Figure 6. Tropospheric column precursor trends in South America and its subregions for the 2005–2021 period (except for methane: 2005–2020). Panels show trends of tropospheric column NO in pmol mol^{-1} decade^{-1} (first row), NO_2 in pmol mol^{-1} decade^{-1} (second row), CH_2O in pmol mol^{-1} decade^{-1} (third row), CO in nmol mol^{-1} decade^{-1} (fourth row) and CH_4 in nmol mol^{-1} decade^{-1} (fifth row). Error bars show confidence interval ($\pm$2 sigma). Colours indicate reliability.

5. Key policy-relevant messages

In line with the scientific scope of TOAR-II, the messages presented below are not policy prescriptive.

(a) Ozone management and infrastructure required

Systematic monitoring of VOCs is crucial for determining the contributions of anthropogenic and biogenic reactive species to ozone trends and should be considered as a routine measurement in South America, particularly in ozone non-attainment areas, where mitigation strategies must be designed according to the local ozone formation regime based on the understanding of the VOC to NO_x ratio.

The progressive regulation of ozone across South America since the 1990s has been key to assessing exposure levels in urban areas. However, the performance of monitoring networks and data quality varies across countries and within cities of the same country. While environmental infrastructure and agencies are now relatively mature, further progress is needed towards collaborative regional networks. Such networks could facilitate quantitative activities, such as intercomparison campaigns, to evaluate environmental technologies and ensure the collection of high-quality data, while also enhancing transparency and public accountability. Similar efforts are required to harmonize datasets and adopt standardized methods for trend estimation and change-point detection, which are fundamental for evaluating the effectiveness of interventions and anticipating emission mitigation strategies.

Another pressing challenge is sustaining long-term measurements in remote regions to detect changes in atmospheric composition and better interpret the climate system. To date, these initiatives have been largely driven by international institutions, such as the WMO and NOAA, in collaboration with local academic and governmental partners. Expanding observational capacity

Downloaded from royalsocietypublishing.org/rsta/article-pdf/doi/10.1098/rsta.2025.0273/6174208/rsta.2025.0273.pdf
by guest
on 09 November 2026

through supersite stations in regions of hemispheric importance, with stronger involvement of national scientific and environmental agencies, will be essential.

While substantial progress has been made in estimating precursor emissions from satellites, satellite-based estimates of near-surface ozone remain subject to considerable uncertainties, which limit their direct applicability for environmental policy. Chemical reanalyses offer a robust framework for integrating multiple observational datasets, particularly in regions where ground-based measurements are scarce. Nevertheless, biases in the estimation of surface mixing ratios persist owing to residual model errors and insufficient observational constraints [5,51,52]. Expanding ground-based monitoring networks, together with the deployment of geostationary satellites dedicated to South America, would strengthen the evaluation of existing data products and, through assimilation with low-Earth-orbiting satellites, enhance their robustness and policy relevance.

Furthermore, future progress in South America will also depend on improving emission inventories and integrating them with modelling systems. To maximize their policy relevance, chemical transport models should be applied in coordinated regional frameworks, combining bottom-up and satellite-based inventories with assimilation techniques to generate South America-specific chemical reanalyses. Such an integrated approach, linking inventories, observations and models, would provide a more robust foundation for trend attribution, enable harmonized assessments across national borders and help anticipate the ozone response to emerging policy interventions and climate-driven changes.

(b) Mitigation of ozone precursors and adaptation to ozone pollution

Mitigating ozone precursors requires a systemic approach, as their main regional sources include both anthropogenic and biogenic sources. Effective and sustained mitigation requires intersectoral efforts, particularly for precursors that are intertwined with fossil fuel production, extreme meteorological events and agricultural activities.

We identified an adverse scenario in mid-latitude urban environments for ozone exposure, where upward background methane can substantially enhance ozone formation, and biogenic isoprene emissions increase during warmer summers. Under this context, it is crucial to strengthen climate resilience in cities by explicitly addressing heat-ozone compound risks, with a focus on reducing ozone exposure to prevent chronic diseases and premature deaths.

6. Conclusion

In South America, we identified the west and east subregions as those with the highest tropospheric column ozone levels during the 2005–2021 period, while the northwest and south subregions exhibited the lowest levels for the same period. The tropospheric column ozone median ($\pm 2\sigma$) obtained from CAMSRA and TCR-2 reanalysis ranged in the northwest, east, west and south between 39 [±8]–42 [±8], 46 [±11] –49 [±9], 47 [±13]–48 [±10] and 38 [±11]–40 [±7] nmol mol^{-1}, respectively.

According to CAMSRA and TCR-2, nitric oxide and nitrogen dioxide are more abundant in the lower troposphere, particularly over urban areas, except for the sparsely populated southern subregion. Carbon monoxide and formaldehyde are most abundant in the northwest subregion, especially in the lower troposphere over wetland-rich areas. A similar horizontal distribution was observed for methane, which also showed enhancements over the east subregion.

Tropospheric column ozone trends diverge between combined satellite products and reanalysis in South America (2005–2021), indicating the need for future efforts to reconcile these ozone tropospheric products. Thus, combined satellite products indicate a negative trend in tropospheric column ozone with low certainty. By contrast, CAMSRA and TCR-2 reanalyses exhibit a positive trend of +0.85 [±0.70] and +0.55 [±0.85] nmol mol^{-1} decade^{-1}, respectively, with high certainty. The increase detected by both reanalyses was largely driven by the western subregion, where precursor availability and elevated terrain (approx. 23°–35° S) favour ozone formation and stratosphere–troposphere exchange, respectively.

Downloaded from royalsocietypublishing.org/rsta/article-pdf/doi/10.1098/rsta.2025.0273/6174208/rsta.2025.0273.pdf
by guest
on 09 November 2026

CAMSRA and TCR-2 detected consistent positive trends in the middle tropospheric column ozone (free troposphere) over the west subregion, exhibiting +2.5 [±1.2] and +1.5 [±0.9] nmol mol^{-1} $decade^{-1}$, both with very high certainty. In the northwest, the middle tropospheric column ozone shows very low certainty trends. In the east, the trends diverge from very low certainty (CAMSRA) to medium certainty (+1.1 [±1.1] nmol mol^{-1} $decade^{-1}$) for TCR-2. In the south, CAMSRA identified a high certainty positive trend, while a low certainty trend was found for TCR-2.

Tropospheric column trends in nitric oxide and nitrogen dioxide also reflect differences within subregions and tropospheric partial columns. For these two species, the downward trends detected by CAMSRA are primarily driven by changes in the upper tropospheric column over the northwest. Conversely, the low certainty positive trend in nitrogen dioxide over South America is primarily driven by the lower tropospheric column over the west.

Methane exhibits a very high certainty positive trend in South America (+66 [±4.6] nmol mol^{-1} $decade^{-1}$), confirmed across all subregions between 2005 and 2020, with an accumulated methane of 1.1×10^2 nmol mol^{-1}. Carbon monoxide exhibits a negative but low certainty trend, whereas the positive trend in formaldehyde of +44 [±1.1] pmol mol^{-1} $decade^{-1}$ is primarily driven by the northwest subregion, with very high certainty.

Over South America, the CAM4-Chem model estimated the contribution of ozone precursors to tropospheric column ozone mixing ratios at 42 nmol mol^{-1} (2005–2018). Reactive carbon-tagged simulations identified methane as the main driver (41%, 17 nmol mol^{-1}). While nitrogen oxides-tagged simulations identified anthropogenic nitrogen oxides (31%, 13 nmol mol^{-1}), stratospheric transport (28%, 12 nmol mol^{-1}) and lightning (28%, 12 nmol mol^{-1}) as the most significant precursors (and sources).

At the subregional scale, biogenic VOCs play a major role in the northwest. Similarly, lightning-produced nitrogen oxides are an important source of ozone. However, the negative trend in lightning activity, a proxy for convective processes, indicates a decline for this ozone source. Stratospheric ozone transport is strongest in the west and south, particularly over the Andes. In the south subregion, nitrous oxide, capable of reaching the stratosphere and producing ozone precursors, contributes about 10% (4 nmol mol^{-1}) of ozone.

Ethics. This work did not require ethical approval from a human subject or animal welfare committee.

Data accessibility. Data used in this research are available in the following public data repositories, MERRA2 [43]: https://datapub.fz-juelich.de/slcs/tropopause/, TCR2 [32]: https://daac.gsfc.nasa.gov/datasets?project=TROPESS, CAMSRA [30,31]: https://ads.atmosphere.copernicus.eu/, HEGIFTOM [13]: https://hegiftom.meteo.be/datasets/tropospheric-ozone-columns-trocs, CAM4-Chem [53], The global 5° × 5° combined satellite data [26] are accessible from https://doi.org/10.18758/39zdhztg.

Supplementary material is available online [54].

Declaration of AI use. We have not used AI-assisted technologies in creating this article.

Authors' contributions. R.S.: conceptualization, formal analysis, investigation, methodology, writing—original draft, writing—review and editing; H.W.: conceptualization, investigation, writing—review and editing; K.M.: conceptualization, data curation, investigation, methodology, writing—review and editing; T.A.: data curation, investigation, methodology, writing—review and editing; T.B.: conceptualization, methodology, writing—review and editing; C.O.: data curation, formal analysis, investigation, methodology, visualization, writing—review and editing; L.C.: data curation, formal analysis, investigation, methodology, visualization, writing—review and editing; D.H.: data curation, investigation, methodology, writing—review and editing; V.S.: data curation, investigation, methodology, writing—review and editing; G.D.: data curation, investigation, methodology, writing—review and editing; P.L.: conceptualization, writing—review and editing.

All authors gave final approval for publication and agreed to be held accountable for the work performed therein.

Conflict of interest declaration. We declare we have no competing interests.

Funding. This work has been supported by the National Aeronautics and Space Administration (NASA). This research was supported by the NSF National Center for Atmospheric Research (NCAR), which is a major facility sponsored by the U.S. National Science Foundation under Cooperative Agreement No. 1852977. Part of this research was carried out at the Jet Propulsion Laboratory, California Institute of Technology, under contract with the National Aeronautics and Space Administration (80NM0018D0004). We acknowledge the

Downloaded from royalsocietypublishing.org/rsta/article-pdf/doi/10.1098/rsta.2025.0273/6174208/rsta.2025.0273.pdf
by guest
on 09 November 2026

use of data products from NASA (Aura and EOS Terra and Aqua satellite missions). We also acknowledge the support of the NASA Atmospheric Composition: Aura Science Team Program (19-AURAST19-0044), Earth Science U.S. Participating Investigator program (22-EUSPI22-0005), ACMAP (22-ACMAP22-0013) and the NASA TROPESS project. IASI is a joint mission of EUMETSAT and the Centre National d'Etudes Spatiales (CNES). The authors acknowledge the AERIS data infrastructure for providing access to the IASI-CDR Level 2 ozone data used in this study, as well as the IASI+GOME2 multispectral ozone products. The authors also acknowledge ULB-LATMOS for the development of the retrieval algorithms and EUMETSAT Atmospheric Composition Satellite Application Facility for ozone data production. The authors further acknowledge the support for the IASI+GOME2 ozone product development and production from CNES (via the TOSCA program), Université Paris-Est Créteil (UPEC), AERIS and Centre National de la Recherche Scientifique (CNRS-INSU). This work also benefited from satellite data products developed within projects supported by the European Space Agency (ESA), including the OREGANO project. This research has been partially supported by ANID (National Agency for Research and Development of Chile) grant no. ANID/FONDEQUIP/EQM190064 and ANID/FONDECYT/1241459. Additional support was provided by CR2, based at the University of Chile, through the Actividades de Interés Nacional (AIN) program. Powered@NLHPC: This research was partially supported by the supercomputing infrastructure of the NLHPC (CCSS210001).

Acknowledgments. The authors acknowledge the guidance and support of the International Global Atmospheric Chemistry (IGAC) project. The Tropospheric Ozone Assessment Report, Phase II (TOAR-II), was conducted as a sponsored IGAC Activity. The authors thank Anne Thompson, Ryan Stauffer and Debra Kollonige for their recommendations to improve this assessment paper.

References

1. Szopa S *et al.* 2023 Short-lived climate forcers. In *Climate change 2021 – the physical science basis*, pp. 817–922. Cambridge, UK: Cambridge University Press.
2. Gaudel A *et al.* 2018 Tropospheric ozone assessment report: present-day distribution and trends of tropospheric ozone relevant to climate and global atmospheric chemistry model evaluation. *Elem. Sci. Anth.* **6**, 39. (doi:10.1525/elementa.291)
3. Mills G *et al.* 2018 Tropospheric ozone assessment report: present-day tropospheric ozone distribution and trends relevant to vegetation. *Elem. Sci. Anth.* **6**, 47. (doi:10.1525/elementa.
302)
4. Fleming ZL *et al.* 2018 Tropospheric ozone assessment report: present-day ozone distribution and trends relevant to human health. *Elem. Sci. Anth.* **6**, 12. (doi:10.1525/elementa.273)
5. Jones DBA *et al.* 2025 Assessment of regional and interannual variations in tropospheric ozone in chemical reanalyses. *Atmos. Chem. Phys.* **26**, 6655–6682. (doi:10.5194/egusphere-2024-3759)
6. Cooper OR *et al.* 2020 Multi-decadal surface ozone trends at globally distributed remote locations. *Elem. Sci. Anth.* **8**, 23. (doi:10.1525/elementa.420)
7. Gulev S *et al.* 2023 Changing state of the climate system. In *Climate change 2021 – the physical science basis*, pp. 287–422. Cambridge, UK: Cambridge University Press.
8. Garstang M *et al.* 1990 The amazon boundary-layer experiment (ABLE 2B): a meteorological perspective. *Bull. Amer. Meteorol. Soc.* **71**, 19–32. (doi:10.1175/1520-0477(1990)071⟨0019:TABLEA⟩2.0.CO;2)
9. Harriss RC. 1988 The amazon boundary layer experiment (ABLE 2A): dry season 1985. *J. Geophys. Res.* **93**, 1351–1360. (doi:10.1029/JD093iD02p01351)
10. Seguel RJ *et al.* 2024 Changes in South American surface ozone trends: exploring the influences of precursors and extreme events. *Atmos. Chem. Phys.* **24**, 8225–8242. (doi:10.5194/acp-24-8225-2024)
11. Gaudel A *et al.* 2024 Tropical tropospheric ozone distribution and trends from in situ and satellite data. *Atmos. Chem. Phys.* **24**, 9975–10 000. (doi:10.5194/acp-24-9975-2024)
12. Chang K-L, Schultz MG, Koren G, Selke N. 2023 Guidance note on best statistical practices for TOAR analyses. (doi:48550/arXiv.2304.14236)
13. Van Malderen R *et al.* 2025 Global ground-based tropospheric ozone measurements: reference data and individual site trends (2000–2022) from the TOAR-II/HEGIFTOM project. *Atmos. Chem. Phys.* **25**, 7187–7225. (doi:10.5194/acp-25-7187-2025)

Downloaded from royalsocietypublishing.org/rsta/article-pdf/doi/10.1098/rsta.2025.0273/6174208/rsta.2025.0273.pdf
by guest
on 09 November 2026

14. Thompson AM *et al.* 2025 Tropical tropospheric ozone trends (1998 to 2023): new perspectives from SHADOZ, IAGOS and OMI/MLS observations. *Atmos. Chem. Phys.* **25**, 18 475–18 507. (doi:10.5194/acp-25-18475-2025)
15. Elshorbany Y *et al.* 2024 Tropospheric ozone precursors: global and regional distributions, trends, and variability. *Atmos. Chem. Phys.* **24**, 12 225–12 257. (doi:10.5194/acp-24-12225-2024)
16. Riese M, Ploeger F, Rap A, Vogel B, Konopka P, Dameris M, Forster P. 2012 Impact of uncertainties in atmospheric mixing on simulated UTLS composition and related radiative effects. *J. Geophys. Res. Atmos.* **117**, D16305. (doi:10.1029/2012JD017751)
17. Škerlak B, Sprenger M, Wernli H. 2014 A global climatology of stratosphere-troposphere exchange using the ERA-Interim data set from 1979 to 2011. *Atmos. Chem. Phys.* **14**, 913–937. (doi:10.5194/acp-14-913-2014)
18. Lan X, Thoning KW, Dlugokencky EJ. 2025 *Trends in globally-averaged CH4, N2O, and SF6 determined from NOAA Global Monitoring Laboratory measurements*. Version 2025-11. Earth System Research Laboratories, Global Monitoring Laboratory. (doi:10.15138/P8XG-AA10)
19. Glatthor N *et al.* 2015 Seasonal and interannual variations in HCN amounts in the upper troposphere and lower stratosphere observed by MIPAS. *Atmos. Chem. Phys.* **15**, 563–582. (doi:10.5194/acp-15-563-2015)
20. Johansson S, Wetzel G, Friedl-Vallon F, Glatthor N, Höpfner M, Kleinert A, Neubert T, Sinnhuber BM, Ungermann J. 2022 Biomass burning pollution in the South Atlantic upper troposphere: GLORIA trace gas observations and evaluation of the CAMS model. *Atmos. Chem. Phys.* **22**, 3675–3691. (doi:10.5194/acp-22-3675-2022)
21. Lichtig P, Gaubert B, Emmons LK, Jo DS, Callaghan P, Ibarra-Espinosa S, Dawidowski L, Brasseur GP, Pfister G. 2024 Multiscale CO budget estimates across South America: quantifying local sources and long range transport. *J. Geophys. Res. Atmos.* **129**, e2023JD040434. (doi:10.1029/2023JD040434)
22. Holanda BA *et al.* 2023 African biomass burning affects aerosol cycling over the Amazon. *Commun. Earth Environ.* **4**, 154. (doi:10.1038/s43247-023-00795-5)
23. Lim E-P *et al.* 2021 The 2019 southern hemisphere stratospheric polar vortex weakening and its impacts. *Bull. Amer. Meteorol. Soc.* **102**, E1150–E1171. (doi:10.1175/BAMS-D-20-0112.1)
24. Seguel RJ *et al.* 2025 Hemispheric differences in ozone across the stratosphere–troposphere exchange region. *Atmos. Chem. Phys.* **25**, 8553–8573. (doi:10.5194/acp-25-8553-2025)
25. Abrahamsen EP *et al.* 2020 Antarctica and the Southern Ocean. *Bull. Amer. Meteorol. Soc.* **101**, S287–S320. (doi:10.1175/BAMS-D-20-0090.1)
26. Hubert D *et al.* 2026 Tropospheric ozone assessment report II: past and present tropospheric ozone using satellite observations. *Phil. Trans. R. Soc. A* **384**, 20250274. (doi:10.1098/rsta.2025-0274)
27. Butler T, Lupascu A, Coates J, Zhu S. 2018 TOAST 1.0: tropospheric ozone attribution of sources with tagging for CESM 1.2.2. *Geosci. Model Dev.* **11**, 2825–2840. (doi:10.5194/gmd-11-2825-2018)
28. Nalam A, Lupaşcu A, Ansari T, Butler T. 2025 Regional and sectoral contributions of NOx and reactive carbon emission sources to global trends in tropospheric ozone during the 2000–2018 period. *Atmos. Chem. Phys.* **25**, 5287–5311. (doi:10.5194/acp-25-5287-2025)
29. Ansari T, Nalam A, Lupaşcu A, Hinz C, Grasse S, Butler T. 2025 Explaining trends and changing seasonal cycles of surface ozone in North America and Europe over the 2000–2018 period: a global modelling study with NO *x* and VOC tagging. *Atmos. Chem. Phys.* **25**, 16 833–16 876. (doi:10.5194/acp-25-16833-2025)
30. Inness A *et al.* 2019 The CAMS reanalysis of atmospheric composition. *Atmos. Chem. Phys.* **19**, 3515–3556. (doi:10.5194/acp-19-3515-2019)
31. Agustí-Panareda A *et al.* 2023 Technical note: the CAMS greenhouse gas reanalysis from 2003 to 2020. *Atmos. Chem. Phys.* **23**, 3829–3859. (doi:10.5194/acp-23-3829-2023)
32. Miyazaki K *et al.* 2020 Updated tropospheric chemistry reanalysis and emission estimates, TCR-2, for 2005–2018. *Earth Syst. Sci. Data* **12**, 2223–2259. (doi:10.5194/essd-12-2223-2020)
33. Granier C *et al.* 2011 Evolution of anthropogenic and biomass burning emissions of air pollutants at global and regional scales during the 1980–2010 period. *Clim. Change* **109**, 163–190. (doi:10.1007/s10584-011-0154-1)
34. Kaiser JW *et al.* 2012 Biomass burning emissions estimated with a global fire assimilation system based on observed fire radiative power. *Biogeosciences* **9**, 527–554. (doi:10.5194/bg-9-527-2012)

Downloaded from royalsocietypublishing.org/rsta/article-pdf/doi/10.1098/rsta.2025.0273/6174208/rsta.2025.0273.pdf
by guest
on 09 November 2026

35. Guenther AB, Jiang X, Heald CL, Sakulyanontvittaya T, Duhl T, Emmons LK, Wang X. 2012 The model of emissions of gases and aerosols from nature version 2.1 (MEGAN2.1): an extended and updated framework for modeling biogenic emissions. *Geosci. Model Dev.* **5**, 1471–1492. (doi:10.5194/gmd-5-1471-2012)
36. Janssens-Maenhout G *et al.* 2015 HTAP_v2.2: a mosaic of regional and global emission grid maps for 2008 and 2010 to study hemispheric transport of air pollution. *Atmos. Chem. Phys.* **15**, 11 411–11 432. (doi:10.5194/acp-15-11411-2015)
37. Graedel TE *et al.* 1993 A compilation of inventories of emissions to the atmosphere. *Global Biogeochem. Cycles* **7**, 1–26. (doi:10.1029/92GB02793)
38. Crippa M *et al.* 2023 The HTAP_v3 emission mosaic: merging regional and global monthly emissions (2000-2018) to support air quality modelling and policies. *Earth Syst. Sci. Data* **15**, 2667–2694. (doi:10.5194/essd-15-2667-2023)
39. van der Werf GR *et al.* 2010 Global fire emissions and the contribution of deforestation, savanna, forest, agricultural, and peat fires (1997–2009). *Atmos. Chem. Phys.* **10**, 11 707–11 735. (doi:10.5194/acp-10-11707-2010)
40. Sindelarova K, Markova J, Simpson D, Huszar P, Karlicky J, Darras S, Granier C. 2021 Copernicus atmosphere monitoring service global biogenic VOC emissions version 3.0 (CAMS-GLOBBIO v3.0). *ECCAD*. (doi:10.24380/xs64-gj42)
41. Tilmes S *et al.* 2015 Description and evaluation of tropospheric chemistry and aerosols in the Community Earth System Model (CESM1.2). *Geosci. Model Dev.* **8**, 1395–1426. (doi:10.5194/gmd-8-1395-2015)
42. Molod A, Takacs L, Suarez M, Bacmeister J. 2015 Development of the GEOS-5 atmospheric general circulation model: evolution from MERRA to MERRA2. *Geosci. Model Dev.* **8**, 1339–1356. (doi:10.5194/gmd-8-1339-2015)
43. Hoffmann L, Spang R. 2022 An assessment of tropopause characteristics of the ERA5 and ERA-interim meteorological reanalyses. *Atmos. Chem. Phys.* **22**, 4019–4046. (doi:10.5194/acp-22-4019-2022)
44. Lamarque J-F *et al.* 2012 CAM-chem: description and evaluation of interactive atmospheric chemistry in the Community Earth system model. *Geosci. Model Dev.* **5**, 369–411. (doi:10.5194/gmd-5-369-2012)
45. Emmons LK, Hess PG, Lamarque J-F, Pfister GG. 2012 Tagged ozone mechanism for MOZART-4, CAM-chem and other chemical transport models. *Geosci. Model Dev.* **5**, 1531–1542. (doi:10.5194/gmd-5-1531-2012)
46. Butler T, Lupascu A, Nalam A. 2020 Attribution of ground-level ozone to anthropogenic and natural sources of nitrogen oxides and reactive carbon in a global chemical transport model. *Atmos. Chem. Phys.* **20**, 10 707–10 731. (doi:10.5194/acp-20-10707-2020)
47. Seguel RJ, Garreaud R, Muñoz R, Bozkurt D, Gallardo L, Opazo C, Jorquera H, Castillo L, Menares C. 2023 Volatile organic compounds measured by proton transfer reaction mass spectrometry over the complex terrain of Quintero Bay, Central Chile. *Environ. Pollut.* **330**, 121759. (doi:10.1016/j.envpol.2023.121759)
48. Lelieveld J, Crutzen PJ. 1991 The role of clouds in tropospheric photochemistry. *J. Atmos. Chem.* **12**, 229–267. (doi:10.1007/BF00048075)
49. East JD *et al.* 2024 Interpreting the seasonality of atmospheric methane. *Geophys. Res. Lett.* **51**, e2024GL108494. (doi:10.1029/2024GL108494)
50. Stauffer RM *et al.* 2024 Dynamical drivers of free-tropospheric ozone increases over equatorial Southeast Asia. *Atmos. Chem. Phys.* **24**, 5221–5234. (doi:10.5194/acp-24-5221-2024)
51. Miyazaki K, Marchetti Y, Montgomery J, Lu S, Bowman K. 2025 Identifying drivers of surface ozone bias in global chemical reanalysis with explainable machine learning. *Atmos. Chem. Phys.* **25**, 8507–8532. (doi:10.5194/acp-25-8507-2025)
52. Wang H *et al.* 2025 Intercomparison of global ground-level ozone datasets for health-relevant metrics. *Atmos. Chem. Phys.* **25**, 15 969–15 990. (doi:10.5194/acp-25-15969-2025)
53. Ansari T. 2025 3D gridded dataset: NOx and VOC regional/sectoral source contributions to monthly averaged tropospheric ozone over South America for 2000–2018. Zenodo. (doi:10.5281/zenodo.18089420)
54. Seguel R 2026 Supplementary material from: Tropospheric Ozone Assessment Report II: South America regional analysis. Figshare. (doi:10.6084/m9.figshare.c.8640479)

Downloaded from royalsocietypublishing.org/rsta/article-pdf/doi/10.1098/rsta.2025.0273/6174208/rsta.2025.0273.pdf
by guest
on 09 November 2026